# Raman scattering as an in-situ optical diagnostic

Herman, Irving

Irving P. Herman, "Raman scattering as an in-situ optical diagnostic," Proc. SPIE 1594, Process Module Metrology, Control and Clustering, (1 January 1992); doi: 10.1117/12.56643

SPIE.

Event: Microelectronic Processing Integration, 1991, San Jose, CA, United States

**Invited Paper**

# Raman Scattering as an in situ Optical Diagnostic

Irving P. Herman
Department of Applied Physics
and Microelectronics Sciences Laboratories
Columbia University
New York, NY 10027

## ABSTRACT

Raman microprobe scattering is shown to be a useful non-invasive real-time probe during thin film processing. Applications during laser-assisted processing that are relevant to microelectronics are emphasized.

## 1. INTRODUCTION

Raman scattering is a fast, nondestructive diagnostic of many properties of semiconductors and insulators. Though Raman analysis has been used mostly ex situ after processing,[1] it is equally useful for in situ measurements within a processing chamber and for real-time measurements. This paper will survey the diagnostic capabilities of Raman scattering. Emphasis will be placed on the use of Raman spectroscopy with ~ 1 μm lateral resolution, i.e. Raman microprobe scattering, as a real-time probe during thin film processing. Though many of the examples discussed in this paper involve in situ measurements during localized laser processing, which is also known as direct laser writing, the methods described here are applicable to all forms of thin film processing. The emphasis of this work is on materials and thin film processes of interest to microelectronics.

The identifiable features of a Raman spectrum are the number of observed peaks, their shifts, linewidths and intensities, and the polarization dependence of the peaks.[1] For example, composition can be analyzed from the types of peaks and their shifts. Local temperature can sometimes be determined from Raman peak shifts and widths. The phase of the material, for example the existence of a solid vs. a liquid phase, may be deduced by peak intensities and polarization properties. The identification of crystallinity, such as determining whether the material is a single crystal, polycrystalline or amorphous, and the measurement of grain sizes can be made from Raman linewidths, shifts and polarization properties. Similarly, damage can be identified and assessed by using this information. The magnitude and direction of localized stresses can be measured by looking at Raman shifts and the peak splittings. Also, in some semiconductors doping levels can be measured by looking at altered features in the Raman spectrum caused by doping and by the appearance of new features. Examples of Raman analysis that illustrate most of these capabilities will be presented here.

Raman scattering involves the inelastic scattering of an elementary excitation. In Stokes scattering, an elementary excitation is created and the scattered photon has less energy than the incident laser photon, while in anti-Stokes scattering an excitation is annihilated and the scattered photon has relatively more energy. In most examples of interest here optical phonons are the elementary excitations that are created or destroyed, though in some cases electrons or holes may be scattered or, in superlattices, folded acoustic phonons can be scattered. The rate of scattering Raman photons is $\sim \omega^3\chi^2/\alpha$, where $\omega$ is the laser frequency, $\chi$ is the Raman susceptibility, which has all the dynamical information and as such is sensitive to the polarization of the incident and scattered beams, and $\alpha$ is the absorption coefficient at the laser wavelength (which is usually ~ the absorption coefficient at the Stokes or anti-Stokes wavelength).[2] The lateral spatial resolution is at best $\sim \lambda/2$, where $\lambda$ is the wavelength of the light used, and the depth resolution is $\sim 1/2\alpha$.

Spontaneous Raman signals are usually very weak, so signal enhancement is often necessary. This can be done by working with shorter $\lambda$, making use of resonances in $\chi$, and, when possible, by surface enhanced Raman scattering (SERS)[3] and by taking advantage of optical interference effects.[4] It is also essential to maximize the collection solid angle and data collection times. Collection times can be improved relative to those for photomultiplier detection at the exit slit of a scanning monochromator, by detecting the spectrally dispersed radiation with an intensity-enhanced photodiode array, CCD array, or a position sensitive resistive anode detector (Mepsicron).[5-9] With good signal collection, thin films of

 0-8194-0725-9/92/$4.00

semiconductors and insulators can be analyzed. In some cases, the weak Raman signals from surfaces, monolayers on surfaces, and interfaces can also be studied.[4-6,9-11]

In most studies, visible or ultraviolet lines from a cw argon-ion or krypton-ion laser have been used as the sources of photons. However, pulsed lasers and lasers based on semiconductor diode lasers can be employed if the flux of photons is high enough and if the laser linewidth is sufficiently narrow. Conventional lenses and microscope objectives are often used for photon delivery and collection. Retractable fiber optic-based systems may prove to be very important for real-time monitoring applications. Figure 1 shows a schematic of *in situ* Raman analysis of laser processing and a schematic of the experimental apparatus used in some of the studies described here.

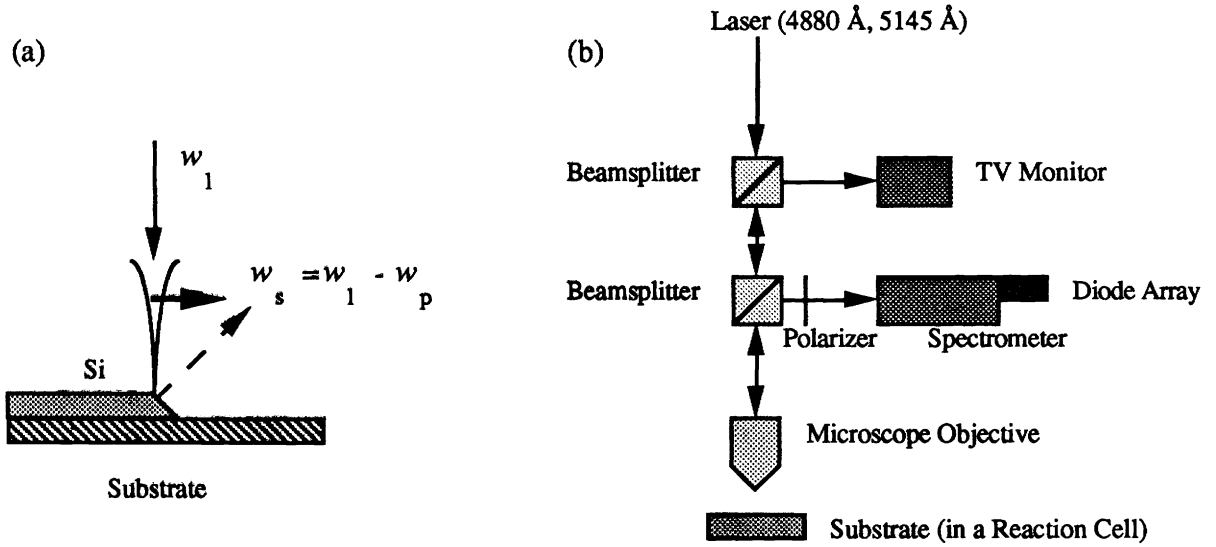


Figure 1. (a) Schematic of a laser-assisted reaction using a scanning, focused laser at frequency $\omega_l$ to heat the substrate and provide photons for Raman scattering, to obtain photons at $\omega_s$. In this example of laser CVD the substrate could be bathed in silane gas. (b) Experimental apparatus used for *in situ* and real-time Raman microprobe analysis during laser-assisted processing.

## 2. RAMAN DIAGNOSTICS

### 2.1 Temperature Probes

For uniformly heated solids the Raman peak can often be represented by a lorentzian with a frequency shift $\omega_p(T)$ and a width $\Gamma_p(T)$ (FWHM) that are functions of temperature T. Because of anharmonicity, $\omega_p$ decreases with T, while $\Gamma_p$ increases with T. Consequently, either the Raman shift or linewidth can be used as a probe of temperature. Using Raman microprobe analysis, the probed region can be ~ $\lambda/2$ wide and $1/2\alpha$ deep. If temperature variations occur over a larger spatial extent, then the local temperature is obtained directly. If there are temperature variations even on such a fine scale, as there can be when tightly focused lasers are used for local heating, the measured profile may not be lorentzian and the observed profile must be deconvoluted, as in Ref. 12, to determine the temperature profile.

The example of laser heating in silicon is examined here. In Figure 2, the zone-center optical phonon frequencies $\omega_p(T)$ and linewidths $\Gamma_p(T)$ for c-Si are plotted up to the melting temperature.[13-15] Near ~ 1000 K the Raman shift varies by ~ – 0.03 $cm^{-1}/K$. In uniformly-heated silicon, remote noninvasive temperature measurements can be made on Si wafers with an accuracy better than 5 K. For a nonuniformly-heated sample, the Raman profile is spatially averaged over the local temperature profile. This has been investigated for the very extreme case of Raman probing of small Si disks on silicon dioxide and sapphire substrates heated by an argon-ion laser that was focused to a ~ 0.6 μm spot size.[12] The temperature profile was probed either by the heating laser or by a second focused laser that was scanned across the disk. One series of spectra is shown in Figure 3a for laser heating and Raman probing of silicon disks on sapphire by the same beam. Since these spectra are averaged over the local temperature, the temperature profile cannot be directly determined from the data in

Figure 2. Instead they were compared with Raman spectrum simulations, where were obtained by using temperature profiles determined by solving the heat flow equation during laser heating. A series of simulated spectra are shown in Figure 3b. Peak temperatures can be determined within ~50 K up to the silicon melting point (1690 K) by comparing these experimental and simulated Raman spectra for these very nonuniform temperature profiles. Sometimes the effects of strains and laser-produced electron/hole pairs can prove to be important in such Raman simulations.

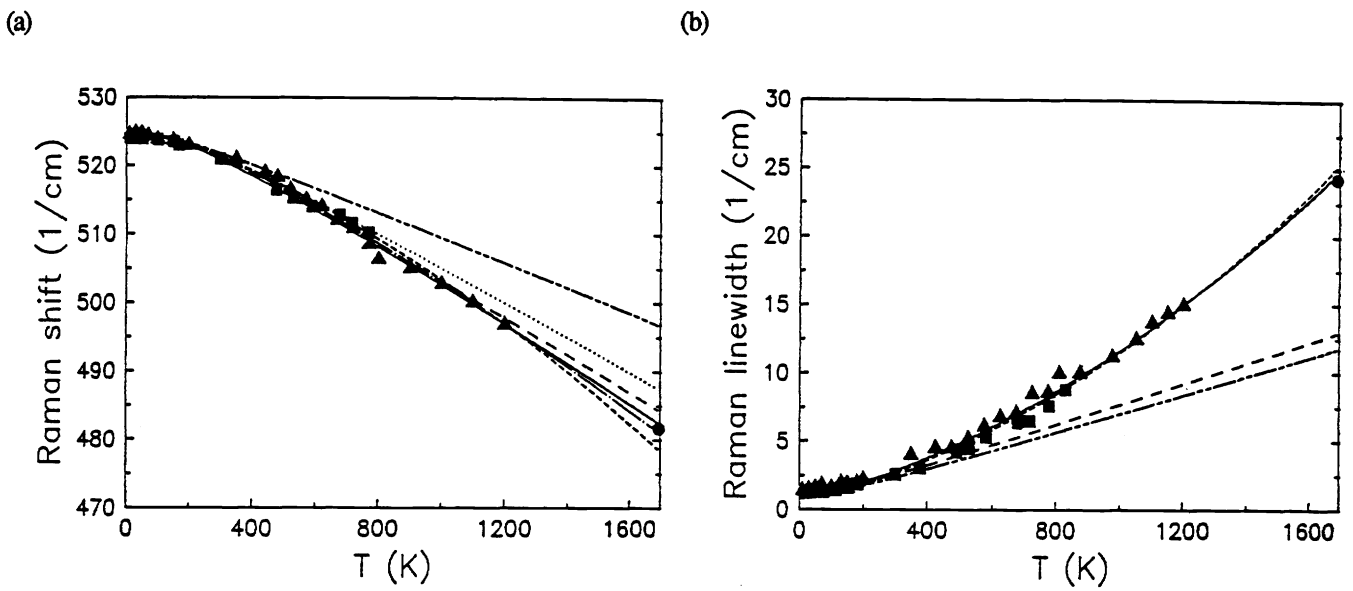


Figure 2. Raman (a) shifts and (b) widths of crystalline silicon vs. temperature T, from Ref. 15. Data are taken from Refs. 13 - 15. Fits of various models of the temperature dependence of phonon energies and decay rates are also shown.

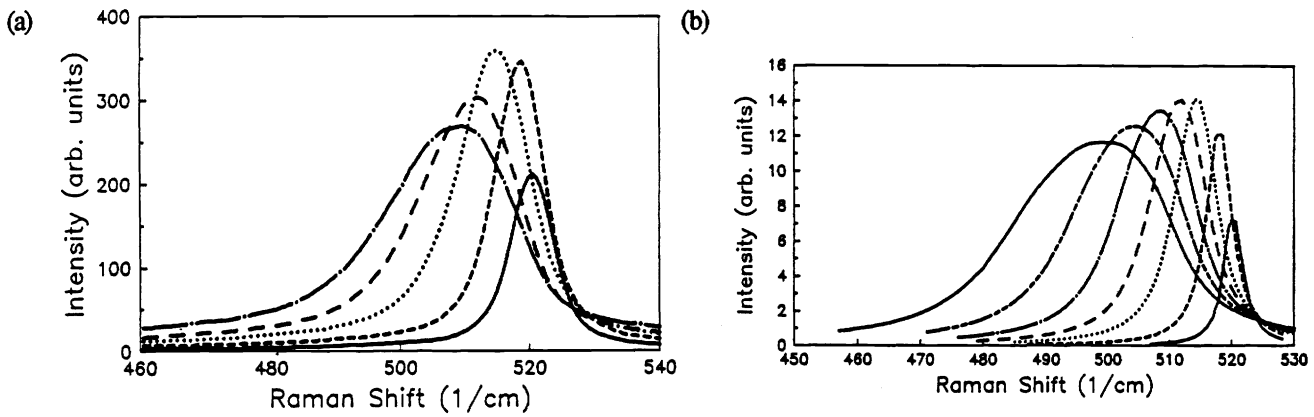


Figure 3. Series of (a) observed and (b) simulated Raman spectra during laser heating of 4-μm diameter silicon disks on a sapphire substrate using a focused laser with 0.6 μm spot size, from Ref. 12. Experiments were conducted with 20, 30, 50, 75 and 85 mW (from right to left) and the simulations assumed 20, 40, 60, 70, 80, 90, and 100 mW.

## 2.2 Phase Changes

One way phase changes can be detected and subsequently followed is by polarization Raman scattering. This has been used to follow laser melting of silicon; similar observations have also made for germanium.[15-17] Si(001) has a strong Raman spectrum in the backscattering configuration when the laser is polarized in the x direction and the analyzed Raman signal is polarized in the y direction, i.e. for the $z(x,y)\bar{z}$ configuration; whereas, the Raman signal vanishes for the $z(x,x)\bar{z}$ configuration. Figure 4 shows how this can be used to determine laser melting of silicon by a static cw laser that is focused

on the surface. In the partially molten silicon formed during laser heating, solid pieces float within the melt and so the crystalline axes of each piece is rotated relative to those of the nonmelted solid. Therefore, using the reference frame of the unmelted solid, there are peaks for both $z(x,x)\bar{z}$ and $z(x,y)\bar{z}$ polarizations at the Raman frequency for solid silicon at its melting point, 482 $cm^{-1}$.[15] Molten silicon has no Raman peak, and the higher $z(x,y)\bar{z}$ peak in this figure represents non-melted material. These spectra were taken during the first 0.5 sec of melting. They can be followed for longer times to examine the flow of the molten material. Also, melting-assisted processes, such as laser etching of Si by chlorine gas, can be followed using this polarization probe.[16,17]

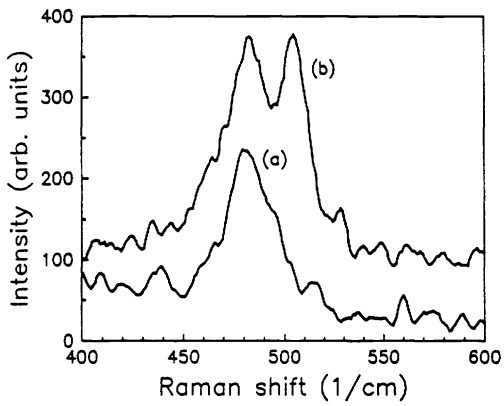


Figure 4. Raman spectra during laser melting of c-Si using (a) $z(x,x)\bar{z}$ and (b) $z(x,y)\bar{z}$ polarizations, from Ref. 15.

## 2.3 Composition

Thin film composition can be followed using Raman scattering. One example of real time analysis of a thin film process is shown in Figure 5, where cw laser-assisted etching of copper films by chlorine gas is followed by Raman microprobe analysis before, during and after this process that uses a scanned argon-ion laser for local heating.[18] Before etching, three peaks from amorphous $Cu_2O$ are seen from the oxidized surface (149, 215 and 646 $cm^{-1}$). During etching, a strong peak near 282 $cm^{-1}$ is seen from nondesorbed $CuCl_2$ products. After etching, in addition to the $CuCl_2$ peaks, a broad peak below ~ 200 $cm^{-1}$ is seen due to CuCl. No evidence of oxidized copper remains. In analogous experiments, real-time Raman scattering demonstrated the growth of $Cu_2O$ during laser-assisted oxidation of copper films.[16]

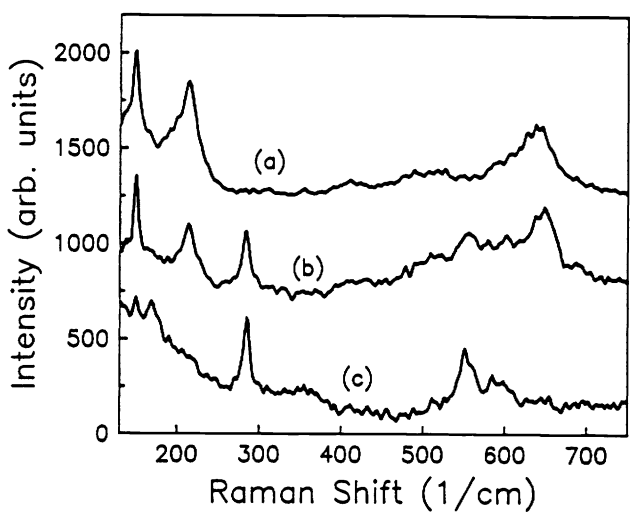


Figure 5. Raman spectra (a) before, (b) during and (c) after laser-assisted etching of a Cu film on glass by chlorine gas, from Ref. 18.

Another example of using Raman scattering for stoichiometry measurements involves determining the Si and Ge fraction in Ge-Si alloys. These alloys have three Raman peaks, a Ge-Ge like mode near 300 $cm^{-1}$, a Ge-Si like mode near 400 $cm^{-1}$, and a Si-Si like mode near 500 $cm^{-1}$.[19] Though the peak shift, width and relative intensity of each of these three peaks depend on composition, the best probe of composition is the Raman shift of the Si-Si peak, which decreases with increasing Ge fraction.[20] This has been used as a composition probe after local laser writing of Ge-Si alloys lines with a focused cw laser beam[21] and after purely thermal and excimer laser-assisted CVD of large-area Ge-Si alloy films, as is shown in Figure 6.[20]

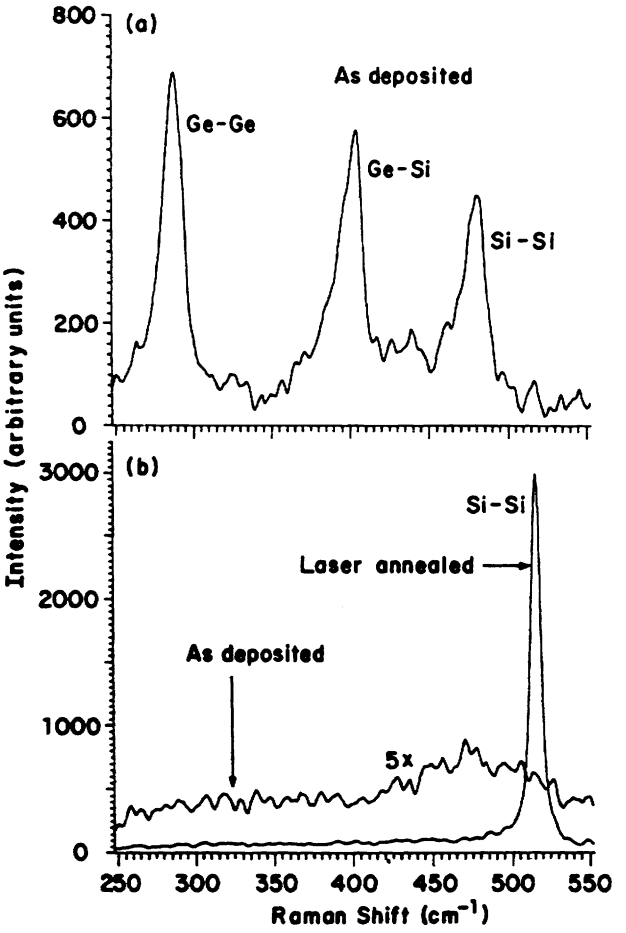


Figure 6. Raman analysis of CVD-grown Ge-Si alloy thin films showing (a) a silicon fraction x = 0.42 of a polycrystalline film and (b) an initially-deposited amorphous film and the annealed polycrystalline film with x = 0.92, from Ref. 20.

Also, in a relatively simple use of Raman scattering as a probe of composition, Magnotta and Herman observed in real time the laser CVD of Si, from silane, on Ge substrates.[22]

## 2.4 Doping

Sometimes the doping of a semiconductor can modify the optical phonon Raman spectrum of a semiconductor, making it a useful diagnostic. These changes can be traced to perturbations due to the dopant atoms and those due to free carriers.[23] For example, new phonon modes can appear because of the substituted atoms. A local Si-B mode is observed near 620 or 644 $cm^{-1}$ due to $^{11}B$ or $^{10}B$ doping of Si (in addition to the first-order peak at 520 $cm^{-1}$ and the two-phonon peak near 620 $cm^{-1}$ in intrinsic Si),[24,25] and a local Ge-Al mode is seen near 360 $cm^{-1}$ in Al-doped Ge (in addition to the 300 $cm^{-1}$ first-order peak in Ge).[26] Also, the dopant atom can lower the symmetry of the crystal and some features that are forbidden in the undoped crystal can become somewhat allowed in the doped crystal. For example, in Raman scattering of

undoped GaAs (001) in backscattering configuration only LO modes are seen. TO modes can also be seen in the Raman spectrum of doped GaAs.[27]

Free carriers can affect Raman scattering of optical phonons either by single particle or collective motion effects.[23] Single particle effects occur at very high doping levels, typically >> $10^{19}$/cc. For example, the Raman lineshapes in heavily p-type doped Si can become very asymmetric, and at high enough doping levels the spectrum can evolve into a peak and a dip. This is due to a Fano-type interference between the Raman scattering of optical phonons and the "electronic" Raman scattering of holes. Collective particle effects can become important at much lower doping levels. In partially ionic crystals, such as GaAs, the LO phonon mode (at frequency $\omega_{phonon}$) and plasmons ($\omega_{plasma}$) couple to form $L_+$ and $L_-$ modes. The electron density n can be determined from the frequencies of these modes since it is related to the plasma frequency as $\sim \sqrt{n}$ .

This diagnostic has been used to determine the width of a line feature in GaAs that was doped by Zn using local laser heating in $Zn(CH_3)_2$.[27] Figure 7 demonstrates that this is accomplished by making use of the decreased crystal symmetry in the doped region.

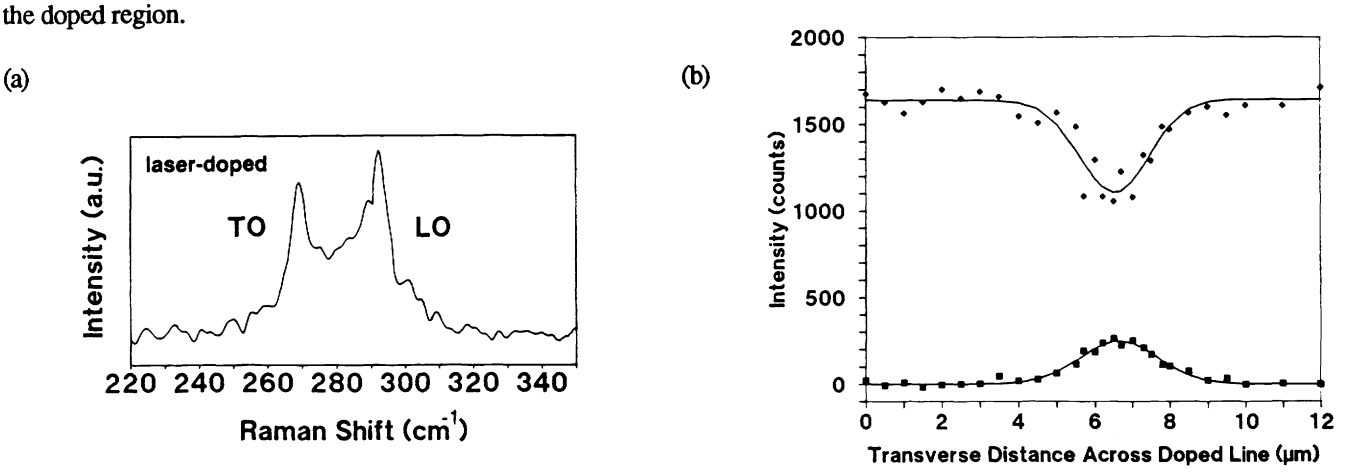


Figure 7. (a) Raman analysis of GaAs that is locally doped by Zn by laser doping, from Ref. 27. In undoped GaAs only the LO mode is seen, while in this heavily doped sample the TO mode is also observed. (b) The intensity of the LO peak (top trace) and TO peak (bottom) across the laser doped line, with a scan 45° across the line.[27] This gives a linewidth of 2.0 μm.

## 2.5 Crystallinity

In first-order Raman scattering from crystals the wavevector q of lattice vibrations is well defined, and only optical phonons near zone-center (q = 0) participate in Raman scattering. In polycrystalline materials of decreasing grain size, phonons increasingly further away from zone center begin to participate and the Raman shift decreases, the width increases, and the profile becomes asymmetric.[28] Polarization Raman scattering can be used to determine grain orientation.[29] For amorphous material, the entire phonon dispersion curve is sampled by Raman scattering, leading to a very broad peak at relatively low frequency. Figure 6b shows that crystallinity can be determined using Raman scattering. The Ge-Si film deposited by CVD[20] initially has the broad spectrum displayed in the figure, which showed that the film was amorphous. This was analyzed *ex situ*, but could have as easily been performed *in situ*. After annealing, the film was re-examined *in situ*. The Raman peak becomes sharp, with contributions mostly near q = 0 zone-center, which indicates (large-grained) polycrystalline material. The closely-related topic of Raman assessment of damage after processing has also been addressed.[30]

## 2.6 Stress

Stress-induced strain perturbs phonon frequencies, thereby perturbing the Raman spectrum. This has been well characterized for zone-center phonons in silicon.[31] In Si, there are three degenerate phonons at q = 0, one LO and two TO phonons. Strain can shift and sometimes split these levels. In backscattering from Si(001), only the LO peak can be seen and strain will shift this peak. For other configurations, scattering from two or three of these phonons can be allowed, and strain can shift and split the Raman spectrum. This has been used to determine stresses in silicon films after patterning or processing in several studies.[32,33] Stress effects can also be important during heating of surfaces by localized beams, and can lead to perturbations of the Raman spectrum.[34]

## 3. CONCLUDING REMARKS

This paper has surveyed the use of Raman scattering to monitor thin film processing *in situ* and in real time. The broad range of properties measured by Raman scattering and its high spatial resolution combine to make it a unique probe. The data obtained from real-time Raman monitoring can be used to understand the physics and chemistry underlying the thin film process and can also be used for real-time monitoring and control.

## 4. ACKNOWLEDGMENTS

The author would like to acknowledge the many valuable contributions made to this work by Hua Tang, Bob Burke, Patrick P. Leong, Gregory Pazionis, Tom Licata, Richard Osgood, and by other collaborators. The Office of Naval Research and IBM are thanked for financial support.

## REFERENCES

1. F. H. Pollak and R. Tsu, SPIE **452**, 26 (1983).

2. W. Hayes and R. Loudon, *Scattering of Light by Crystals*, J. Wiley, New York, 1978.

3. R. P. van Duyne, R. I. Altkorn, and K. L. Haller, IEEE Circuits and Devices, **2(1)**, 61, (1986); R. P. van Duyne, K. L. Haller, R. I. Altkorn, Chem. Phys. Lett. **126**, 190 (1986).

4. R. J. Nemanich, J. M. Thompson, W. B. Jackson, C. C. Tsai, and B. L. Stafford, J. Vac. Sci. Technol. **B1**, 519 (1983).

5. A. Campion, J. K. Brown, and V. M. Grizzle, Surf. Sci. 115, **L153** (1982).

6. J. C. Tsang, Ph. Avouris, and J. R. Kirtley, Chem. Phys. Lett. **94**, 172 (1983).

7. R. K. Chang and M. B. Long, in *Light Scattering in Solids II, Topics in Applied Physics* **50**, edited by M. Cardona and G. Guntherodt, Springer, New York, 1982, p. 179.

8. W. P. Acker, B. Yip, D. H. Leach, and R. K. Chang, J. Appl. Phys. **64**, 2263 (1988).

9. J. C. Tsang, in *Light Scattering in Solids V, Topics in Applied Physics* **66**, edited by M. Cardona and G. Guntherodt, Springer, New York, 1989, p. 233.

10. J. C. Tsang, S. S. Iyer, and S. L. Delage, Appl. Phys. Lett. **51**, 1732 (1987).

11. H. J. Stoltz and G. Abstreiter, J. Vac. Sci. Technol. **19**, 380 (1981).

12. G. D. Pazionis, H. Tang and I. P. Herman, IEEE J. Quantum Electron. **25**, 976 (1989).

13. J. Menendez and M. Cardona, Phys. Rev. **B29**, 2051 (1984).

14. M. Balkanski, R. F. Wallis and E. Haro, Phys. Rev. **B28**, 1928 (1983).

15. H. Tang and I. P. Herman, Phys. Rev. **B43**, 2299 (1991).

16. I. P. Herman, H. Tang, and P. P. Leong, Mat. Res. Soc. Symp. Proc. **201**, 563 (1991).

17. H. Tang and I. P. Herman, submitted for publication.

18. H. Tang and I. P. Herman, J. Vac. Sci. Technol. **A8**, 1608 (1990); Mat. Res. Soc. Symp. Proc. **158**, 331 (1990).

19. M. A. Renucci, J. B. Renucci, and M. Cardona, in *Proceedings of the Conference on Light Scattering in Solids*, edited by M. Balkanski, Flammarion, Paris, 1971, p. 326.

20. H. H. Burke, I. P. Herman, V. Tavitian, and J. G. Eden, Appl. Phys. Lett. **55**, 253 (1989).

21. I. P. Herman and F. Magnotta, J. Appl. Phys. **61**, 5118 (1987).

22. F. Magnotta and I. P. Herman, Appl. Phys. Lett. **48**, 195 (1986).

23. G. Abstreiter, M. Cardona, and A. Pinczuk, in *Light Scattering in Solids IV, Topics in Applied Physics* **54**, edited by M. Cardona and G. Guntherodt, Springer, New York, 1984, p. 5, and references cited therein.

24. M. Chandrasekhar, H. R. Chandrasekhar, M. Grimsditch, and M. Cardona, Phys. Rev. **B22,** 4825 (1980).

25. R. A. Forman, M. I. Bell, and D. R. Myers, J. Appl. Phys. **52**, 4337 (1981).

26. G. Contreras, M. Cardona, and A. Compaan, Solid State Commun. **53**, 857 (1985).

27. T. J. Licata, D. V. Podlesnik, H. Tang, I. P. Herman, R. M. Osgood, Jr., and S. A. Schwarz, J. Vac. Sci. Technol. **A8**, 1618 (1990).

28. I. H. Campbell and P. M. Fauchet, Solid State Commun. **58**, 739 (1986).

29. J. B. Hopkins, L. A. Farrow, and G. J. Fisanik, Appl. Phys. Lett. **44**, 535 (1984).

30. J. Wagner, Appl. Phys. Lett. **52**, 1158 (1988).

31. E. Anastassakis, A. Pinczuk, E. Burstein, F. H. Pollak, and M. Cardona, Sol. State Commun. **8**, 133 (1970).

32. S. R. J. Brueck, B-Y. Tsaur, J. C. C. Fan, D. V. Murphy, T. F. Deutsch, and D. J. Silversmith, Appl. Phys. Lett. **40**, 895 (1982).

33. P. M. Fauchet, I. H. Campbell, and F. Adar, Appl. Phys. Lett. **47**, 479 (1985).

34. L. P. Welsh, J. A. Tuchman, and I. P. Herman, J. Appl. Phys. **64**, 6274 (1988).